Colloquium: Acoustical analogs of condensed-matter problems

J. D. Maynard

Department of Physics, The Pennsylvania State University, University Park, Pennsylvania 16802

(Published 18 May 2001)

As a result of advances in experimental and theoretical physics, many interesting problems have arisen in condensed-matter physics, typically as a result of the quantum-mechanical nature of a system. Areas of interest include Anderson localization, universal conductance fluctuations, normal electron persistent currents, and the properties of quasicrystals. Understanding such systems is challenging because of complications arising from the large number of particles involved, intractable symmetries, the presence of time-dependent or nonlinear terms in the Schrödinger equation, etc. Some progress has been made by studying large scale classical analog experiments which may accurately model the salient quantum-mechanical features of a condensed-matter system. This paper describes research with a number of acoustical systems which have addressed contemporary problems in condensed-matter physics.

CONTENTS

I. INTRODUCTION

A wish that many have is that the central processing unit (CPU) in their computers could go even faster. One way of accomplishing this would be to reduce the size (and the capacitive time constant) of the CPU's components, e.g., the transistors and the wires connecting them. A question which arises in condensed-matter physics is whether or not the laws of physics which hold for the larger components still hold for the smaller ones. For example, for very small connecting wires, is Ohm's Law still valid? Experimental measurements show that, at least at low temperatures, the voltage drop along a small wire is not simply proportional to the current; thus Ohm's Law no longer holds. To understand this at a fundamental level, it would be necessary to solve the Schrödinger wave equation for an electron moving in the potential field of a large number (10^7–10^{23}) of positive ions, a formidable problem. However, if the material were a crystal and the ions were periodic, then it would be sufficient to solve the Schrödinger equation for one unit cell, which can be done to sufficient accuracy for most applications; calculating the band structure for semiconductors, etc., has become routine. Yet there are many important materials, such as amorphous solids, alloys, and small metallic wires, which are highly disordered, so that the problem of solving the wave equation with a large number of nonperiodic scatterers returns. For sufficiently large samples, thermal motion of the ions, i.e., a time-dependent potential field, destroys the wave nature of the electron, permitting a statistical treatment. The Schrödinger wave equation becomes a transport equation, characterized by a mean free path for inelastic scattering, which can be solved, providing a means for dealing with disordered materials. However, several developments in condensed-matter physics have occurred which have again required the solution of the wave equation with nonperiodic scatterers. In one case, small solid grains having quasicrystalline structure were formed. In another case, experimentalists made wires so small that at low temperatures the length of the wire was smaller than the mean free path for inelastic scattering, so that an electron could maintain its phase coherence throughout the wire. A typical experiment might involve wires only 10 nm wide and one micron in length. The study of such small systems, where an electron retains its wave nature, was termed mesoscopic physics. The fundamental problem of waves encountering nonperiodic scatterers dates back at least to Lord Rayleigh, and has been addressed by many outstanding scientists and mathematicians since that time. The resurgence of interest in mesoscopic systems, and long-range phase coherence, has been a current frontier of condensed-matter physics. Interesting problems discussed in this paper involve Anderson localization, the time-dependent and nonlinear Schrödinger equation, normal electron persistent currents, and quasicrystalline symmetry.

In addition to research on mesoscopic systems, another approach to studying long-range phase coherence has been jokingly referred to as ''megascopic'' physics, where phase coherence is maintained for not just one micron, but for ''millions of microns,'' or meters! Such studies employ systems involving classical waves, mechanical or electromagnetic, and might be thought of as

 ©2001 The American Physical Society

"analog computers" for solving the Schrödinger wave equation with complicated potential fields. These classical analog systems may quite accurately model the salient physics of quantum-mechanical systems. For example, in a mesoscopic system, where the sample size is smaller than the mean free path for inelastic scattering, it is satisfactory, for a one-electron model, to solve the time-independent Schrödinger equation:

$$-\frac{\hbar^2}{2m}\nabla^2\psi + V'(\vec{r})\psi = E\psi. \tag{1}$$

The solution ψ describes the behavior of an electron of energy E acted upon by forces with the potential $V'(r)$. The time dependence is $e^{-i(E/\hbar)t}$. Solutions (eigenfunctions) exist only for discrete values of E (eigenvalues); thus the basis for quantum mechanics. By dividing through by $-\hbar^2/2m$, the Schrödinger equation may be rewritten as

$$\nabla^2\psi + [q^2 - V(\vec{r})]\psi = 0, \tag{2}$$

where q is an "eigenvalue parameter," which for the quantum-mechanical system is $\sqrt{2mE/\hbar^2}$, and so related to the energy eigenvalue.

The equation for classical (scalar) waves is

$$\nabla^2\psi - \frac{1}{c^2}\frac{\partial^2\psi}{\partial t^2} = 0, \tag{3}$$

where c is the wave propagation speed. Applying a Fourier transform in time (i.e., assuming a time dependence $e^{-i\omega t}$), and contriving a system where the wave speed varies with position $\vec{r}$, the classical wave equation may be rewritten as

$$\nabla^2\psi + [q^2 - V(\vec{r})]\psi = 0. \tag{4}$$

For the classical system the eigenvalue parameter q is ω/c_0, where ω is an eigenfrequency, or natural frequency, and c_0 is some mean wave propagation speed for the system. Comparing the time dependencies, one sees the quantum and classical relation $E = \hbar\omega$. There are some details omitted in this discussion, such as possible frequency dependence in the classical $V(\vec{r})$ and dispersion (Lifshits, 1964), but in a cleverly designed analog experiment, these may be rendered unimportant. Indeed, often the salient physics in the quantum problem lies in the symmetry of the potential field $V(\vec{r})$, e.g., whether it is periodic, disordered, or quasicrystalline, and other features are unimportant; in this case the classical system may be a very accurate model for the quantum system.

Studies of classical wave mechanical systems have some important advantages over studies of quantum wave mechanical systems. In "megascopic" classical systems all conditions may be precisely controlled or measured. In an experiment one may readily determine eigenvalues and directly measure eigenfunctions, both their amplitude and phase fields. Such measurements have never been made in a quantum system, although attempts with atomic probe microscopes are in progress. The control and observability of the classical analogs may be matched by numerical simulations. However, as will be illustrated in this paper, the classical experiments can reveal aspects of a problem which can be overlooked when a model is being developed for numerical simulation. Furthermore, classical systems may be used to study time-dependent potential fields and nonlinear effects, which are very difficult and time consuming to treat numerically or analytically.

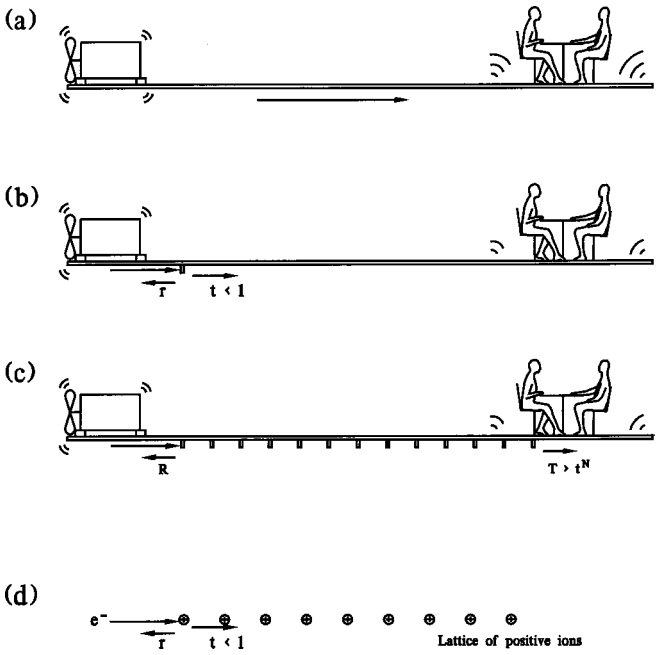

FIG. 1. A problem in noise abatement which motivated research in classical analogs of quantum-mechanical systems.

For classical analog studies using electromagnetic radiation (in the visible range) in disordered dielectric fields, there has been considerable research motivated not only by interest in the fundamental physics, but also by possible applications in fiber-optic devices. However, the classical systems which are the easiest to understand and which provide the most detailed information employ acoustical scalar waves, and this paper will concentrate on these systems.

Interest in acoustical waves in disordered scattering fields was originally motivated by a practical application in noise abatement. Consider a plate, possibly a floorboard in a small aircraft, as illustrated in Fig. 1(a). A source of vibration, such as a motor, generates transverse waves at one end of the plate. The waves travel down the plate, and as the plate vibrates it radiates noise into the air and creates an annoyance. Usually, for structural reasons, a plate will have a rib on it, and that rib reflects the vibration, as shown in Fig. 1(b), so there is less vibration transmitted, and less noise at the other end of the plate. One might reason that if one rib reduces the noise, why not a series of ribs? For ease of manufacture, a periodic array of identical ribs might be used, as in Fig. 1(c). The result would be that instead of a large reduction in noise, the plate would still transmit the waves, at least in certain bands of frequencies. This is analogous to an effect in solid-state physics, for elec-

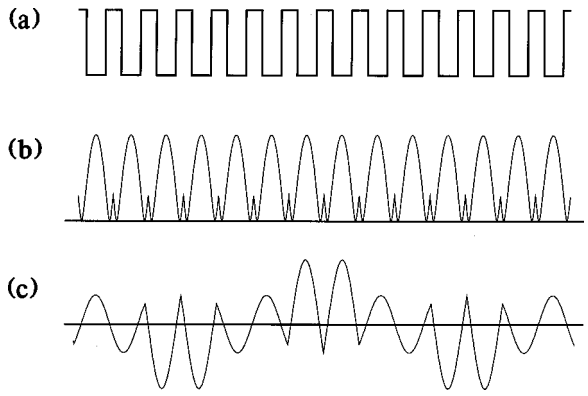

FIG. 2. An example of a periodic potential field and a Bloch wave function. (a) The periodic potential. (b) The modulus of the Bloch wave function, which is also periodic. (c) The Bloch wave function, with phase included.

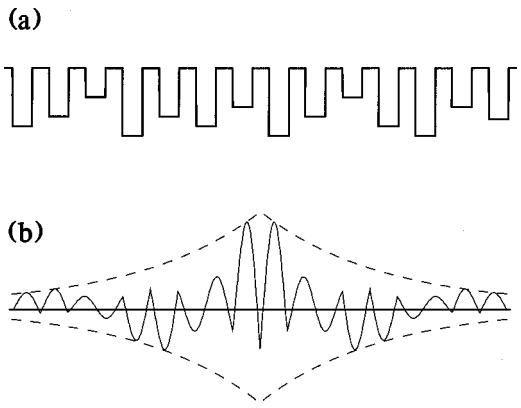

FIG. 3. An example of a disordered potential field and an Anderson localized wave function.

trical conductivity in a metallic crystal.

In a crystalline wire consisting of electrons and fixed positive ions, as illustrated in Fig. 1(d), a classical electron would be very strongly scattered by the ions as it tried to move down the wire, and one would have to conclude that a metal should be a very poor conductor of electricity. That metals are good conductors of electricity is due to two features: (i) the quantum-mechanical electron behaves as a wave, and (ii) in a crystal the ions are arranged periodically. The results for both the waves in the ribbed plate and the electrons in the crystal are consequences of the periodic symmetry of the scattering field and a theorem known in mathematics as Floquet's theorem (Floquet, 1883), and known in physics as Bloch's theorem (Bloch, 1928).

Bloch's theorem states that for a wave equation with a periodic potential (or periodic electric or mechanical impedance), the eigenfunctions are extended; i.e., the wave functions (referred to as Bloch waves) have the form

$$\psi_{k,n}(x) = e^{ikx} U_n(x), \tag{5}$$

where k and n are quantum numbers or mode labels, and $U_n(x)$ is a periodic function with the period of the potential field. Taking the modulus of the wave function $|\psi_{k,n}(x)|$ gives just the periodic function $|U_n(x)|$. Figure 2(a) illustrates a periodic potential, and Fig. 2(b) shows an example of the periodic modulus of a Bloch wave. If the phase e^{ikx} is added, the Bloch wave example has the form illustrated in Fig. 2(c).

If examined in detail, Bloch waves are found to be more complicated than their simple form might suggest. Most introductions to Bloch waves treat periodic systems with periodic boundary conditions, having traveling Bloch wave solutions as illustrated above. However, the e^{ikx} factor does not result in an ordinary traveling wave, because there is a phase contribution from the complex function $U_n(x)$. Also, Bloch "standing waves" are not obtained by replacing the e^{ikx} with $\sin(kx)$ or $\cos(kx)$; they require a bit more manipulation. It is an interesting exercise to write a computer program which gives animated illustrations of Bloch wave packets traveling through a periodic potential.

A key feature of the extended Bloch waves is that they have the same nominal amplitude in each unit cell in the periodic potential field. For a quantum-mechanical electron, this would mean that the electron would have the same probability of being found in any unit cell, which may be expressed by saying that the electron is able to move freely through the array of ions. The analogous situation occurs for the transverse waves in the ribbed plate.

What would happen if the potential field were not periodic, but had some disorder, as illustrated in Fig. 3(a)? One might expect that the previously extended wave function would now have disordered variations in its amplitude as a function of position. Instead, however, the wave function becomes exponentially localized, as illustrated in Fig. 3(b), which shows that at some site the wave function has a maximum amplitude and decreases exponentially away from that site. This phenomenon is called Anderson localization (Anderson, 1958), and was used by P. W. Anderson (1978) and Sir Nevil Mott (1967) to explain the metal-to-insulator transition in disordered metals; this was cited in their Nobel prize in 1977.

The behavior of waves propagating in disordered arrays of scatterers is a fundamental problem which dates back to Lord Rayleigh. Despite the number of distinguished people who have addressed this problem since then, the first rigorous theorem did not appear until 1963, with Furstenberg's theorem (Furstenberg, 1963). This theorem is for one dimension only; a scaling argument suggests the behavior in higher dimensions. An excellent discussion of how disorder leads to exponential localization in one dimension may be found in a paper by Luban and Luscombe (1987). It would be beyond the scope of this paper to delve into the theory of Anderson localization in detail; there are a number of reviews in the literature (Lee and Ramakrishnan, 1985; Altshuler, Lee, and Webb, 1991; Sheng, 1995).

Motivated by the analogy between electrons in periodic or disordered metals and waves in classical acoustical systems such as ribbed plates, an experiment for observing classical Anderson localization was developed. It is described in the next section.

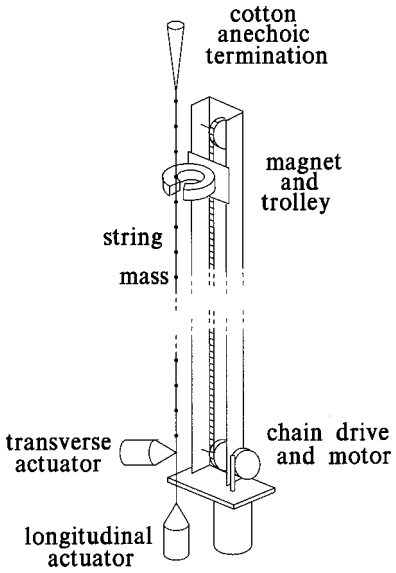

FIG. 4. One-dimensional acoustic Anderson localization experiment, consisting of a steel wire with small masses acting as scatterers.

II. CLASSICAL ANDERSON LOCALIZATION

A. Classical Anderson localization in one dimension

The one-dimensional acoustical system used in the Anderson localization experiment (He and Maynard, 1986) is illustrated in Fig. 4. The wave medium is a long (15-m) 0.178-mm-diameter steel wire suspended vertically; a tension T in the wire is maintained with a weight attached at the lower end. The wave field ψ consists of transverse waves in the wire generated with an electromechanical actuator at one end of the wire. The periodic or nearly periodic potential field V for the wire is provided by small lead masses (with mass $m=249\pm33$ mg) spaced along the wire with an average lattice constant $a=15$ cm; a total of 50 masses is used. The masses are sufficiently small in extent so that the potential V may be approximated as a series of delta functions with strength $m\omega^2/T$; the experiment is an accurate realization of a one-dimensional wave equation with a Kronig-Penny potential field. Experimental measurements and computer simulations have shown that the small variations in the sizes of the masses have negligible effect on the main Anderson localization, as will be discussed later.

Beyond the series of masses the wire continues for a few meters and is then covered with a long taper of cotton which provides an anechoic termination. Running parallel to the wire is a 9-m aluminum beam which acts as a guide for a trolley carrying a "C"-shaped permanent magnet. The magnet is aligned so that the wire passes between its poles, with the lines of force perpendicular to the wire. When the transverse wave field is present along the wire, the magnetic field induces an electromotive force (emf) in the wire which is proportional to the velocity of the wire at the position of the magnet. The emf is measured by grounding one end of the wire and connecting the opposite end (through a fine copper wire) to a preamp and a phase sensitive amplifier referenced to the transverse actuator signal. A motor, gear, and chain system is used to translate the trolley and magnet assembly along the aluminum beam. By monitoring the position of the magnet and the current induced in the wire, the entire wave field along the wire $\psi(x)$, including amplitude and phase, may be recorded.

FIG. 5. Illustration of the wire in the case in which the scatterers have infinite mass; i.e., the wire is clamped at the position of the mass. The eigenfunctions correspond to fitting an integral number of half wavelengths between the clamps.

In the wire-mass system disorder may be introduced by varying the sizes of the masses (alloy-type disorder) or by varying the positions of the masses (liquid-type disorder) (Lifshits, 1938; Ishii, 1973). It was found that the liquid-type disorder, even for very small deviations from periodicity, produced more dramatic localization effects. For example, varying the positions of the masses by less than 1% produced significant localization, while the inherent $\sim$13% variation in the sizes of the commercial lead masses resulted in localization lengths which were much larger than the size of our system. The former variation corresponds to "diagonal disorder," while the latter corresponds to "off-diagonal disorder," which is known to result in much weaker localization than diagonal disorder. To understand this, it would be worthwhile to consider the expected behavior of the system, first assuming a periodic spacing of the masses.

Figure 5 shows the wire, drawn horizontally, in the case where periodically spaced scatterers have infinite mass, so that the wire is clamped at the positions of the masses. The eigenfunctions and eigenvalues are straightforward; the eigenfunctions correspond to fitting an integer number of half wavelengths between the clamps, as indicated in Fig. 5. The eigenvalues (eigenfrequencies) form a harmonic sequence; each section of the wire between the masses may be considered as an isolated local oscillator with sharp eigenvalues, ω_1, ω_2, ω_3, etc., as shown in Fig. 6(a).

In the real system the masses are not infinite, so that as a section of wire moves, the masses and neighboring sections of wire move also; thus each local oscillator is coupled to its nearest neighbors. To understand the effect of the coupling, a system of only two local oscillators may be considered first. Individual states for the two oscillators may be combined to form symmetric and antisymmetric normal modes; with a coupling interaction, these normal modes will have different frequencies (Kittel, 1966). If N local oscillators are coupled, there will be N normal modes and N eigenfrequencies. Thus each of the original sharp eigenfrequencies (ω_1, ω_2, etc.) common to the N oscillators becomes a band of N distinct eigenfrequencies for normal modes of the coupled system. If the strength of the coupling is increased, the spread of the band increases, as illustrated

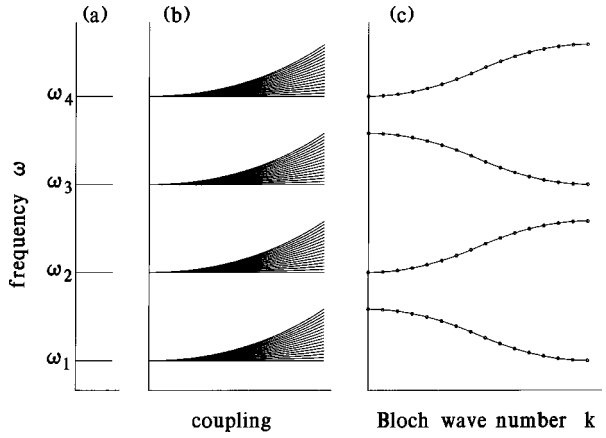

FIG. 6. Illustration of how band structure arises for a periodic system of scatterers along a wire under tension. (a) Frequency spectrum for the case where the scatterers have infinite mass; the sections of the wire between the masses act as isolated local oscillators with sharp eigenfrequencies, ω_1, ω_2, etc. (b) Effect of increasing the coupling between the local oscillators; each sharp eigenfrequency common to N isolated oscillators becomes a band of N distinct frequencies for the normal modes of the coupled system. If the strength of the coupling is increased, the spread of the band increases. (c) For a periodic system, the normal modes comprising each band may be labeled with the Bloch wave number k, providing the classic picture of band structure, as found in solid-state physics.

in Fig. 6(b). For a periodic system, each of the normal modes comprising each band may be labeled with the Bloch wave number k [defined in Eq. (5)], providing the picture of band structure in Fig. 6(c), common in solid-state physics. The different bands may be labeled according to the original sharp local oscillator eigenfrequencies ($\omega_1, \omega_2, \ldots \omega_n$, etc.), and these labels correspond to the Bloch quantum number n in Eq. (5). If N is large, the bands will be densely populated with allowed states (allowed frequencies), while between the bands only evanescent wave states (having imaginary wave numbers) may be excited. Since the evanescent waves do not propagate through the system, they are considered as "unallowed" states. In solid-state physics, the allowed and unallowed regions are "energy bands" and "gaps;" for classical waves (acoustic, microwaves, etc.) they are referred to as "pass bands" and "stop bands."

If the masses are large so that the coupling is weak, then the scatterers have high (nearly unity) reflection coefficients. In the actual experiment, the reflection coefficient was measured as 99.97%. However, since the local oscillators are identical in the periodic system, at particular frequencies all the local oscillators are near resonance; thus any small amount of energy which can get past a scatterer will drive the local oscillator to finite amplitude. This is one way of understanding Bloch waves. In the actual experiment on the periodic system, great effort was taken to ensure that the lengths of wire between the masses were as identical as possible. Having small variations in length would result in local oscillators being off resonance, and this would destroy the Bloch extended wave function; this is a manifestation of the sensitivity to diagonal disorder. By contrast, the masses are strong scatterers, and with variations of 13% in mass they are still strong scatterers. Variations in coupling, as long as it is weak, has little effect on the resonating local oscillators, and thus there is relatively less sensitivity to off-diagonal disorder.

The discussion above also provides a means of understanding how Anderson localization may be readily achieved. If one has a periodic system with local oscillators which are only weakly coupled, then the bands are narrow and the gaps are large. There are states inside the gaps, but they are exponentially decaying evanescent waves which are usually ignored. If one introduces disorder into the periodic system, new states evolve from the original ones, but since the original ones were mostly evanescent waves, the new states have exponentially decaying character. Thus Anderson localization is readily achieved if one begins with local oscillators, with slightly different spectra (diagonal disorder), and couples them weakly. However, this argument is clear for states of the periodic system which were near the band edges; it is still quite remarkable that states in the interior of the band become localized. There will be further discussion of qualitative matters in the section on Anderson localization in higher dimensions.

A very important experimental requirement is that each local oscillator must have low damping, i.e., a high quality factor (Q), so that any energy which is transferred by the weak coupling will, at the right frequency, drive the oscillator to finite amplitude. Similarly, the coupling mechanism should have little damping, so that waves may be transmitted over long distances, permitting the long-range phase coherence required to produce Anderson localization (or other phenomenon related to symmetry).

In an actual Anderson localization experiment, it is essential first to verify Bloch wave behavior by making measurements with a periodic potential field. This is to verify that one can adequately understand and control the parameters in the experiment. The frequency response (band structure) of the system in Fig. 4, with a periodic spacing of the masses, was measured by monitoring the transverse wave amplitude near one end of the series of masses while sweeping the frequency (analogous to electron Fermi energy) of the transverse actuator at the opposite end. Results for the second pass band (which corresponds to fitting approximately one-half wavelength between the masses) are shown in Fig. 7(a). The response shows distinct edges separating the pass band from transmission gaps on either side and approximately 50 eigenfrequencies corresponding to the eigenstates of the 50-site system. The decrease in amplitude at some interior frequencies is due to the fact that the eigenstates are standing Bloch waves, and at some frequencies the detector is near a node in the standing wave. The band is fairly narrow, extending from about 760 to 840 Hz.

By driving the static periodic system at one of the eigenfrequencies and translating the magnet, a Bloch

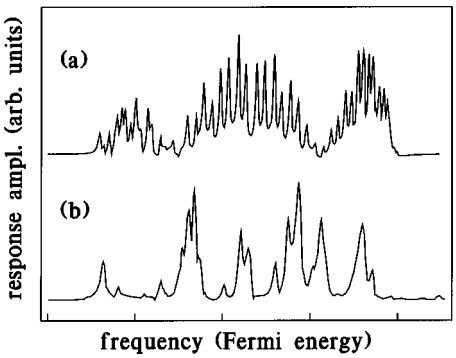

FIG. 7. Response of the wire at one end as a function of the frequency of the transverse actuator at the opposite end (analogous to electron Fermi energy in a conductivity experiment). (a) Periodic potential. (b) 2% random potential.

wave eigenstate is recorded; two examples are presented in Figs. 8(a) and (b), which show the eigenstate amplitude as a function of position along the wire. These eigenstates are clearly extended, and are in qualitative agreement with theoretical Bloch eigenstates.

Several sets of measurements were made with the positions randomly varied within maximum displacements from lattice sites of $0.007a$, $0.01a$, $0.02a$, and $0.05a$. Results with static disorder configurations were in good agreement with computer simulations. Figure 7(b) shows the frequency response of the system with 2% disorder, i.e., with the masses displaced from the periodic lattice sites with a flat random distribution between $\pm 0.02a$. These results show dramatic departure from the

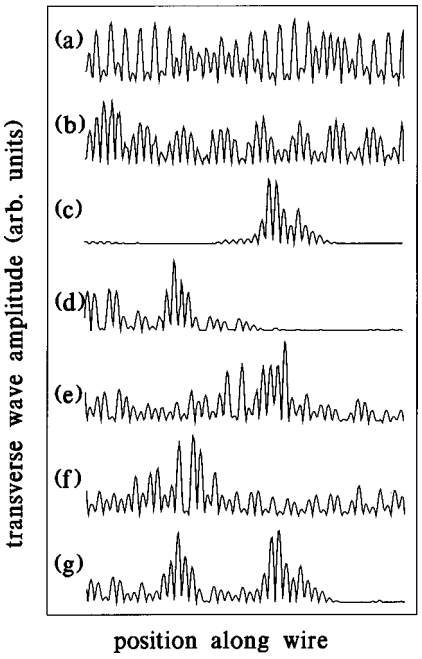

FIG. 8. Eigenstate amplitude as a function of position along the wire. (a) and (b) Bloch wave states. (c)–(f) Eigenstates of the 2% disordered system. (g) Mixing of states (c) and (d) due to the time-dependent potential. The sharp minima in the amplitude [$\sim$ 45 shown in (b)] indicate the positions of the masses, spaced at the lattice constant of 15 cm.

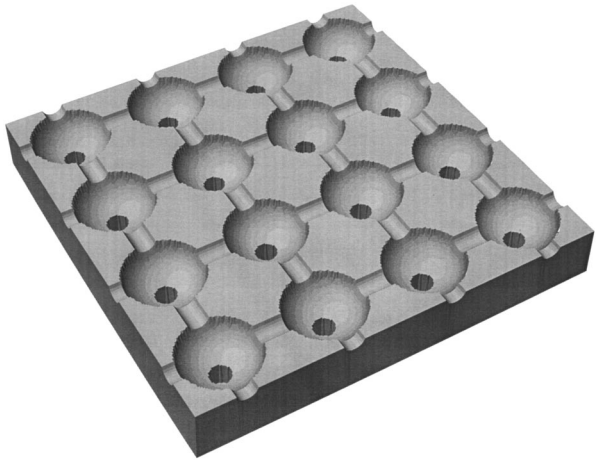

FIG. 9. Illustration of a method for observing classical Anderson localization in two or three dimensions. Stacking plates machined in this pattern result in an array of coupled Helmholtz resonators.

Bloch response in Fig. 7(a). At least one eigenstate appears in the low-frequency gap. Eigenstates corresponding to various peaks in Fig. 7(b) are shown in Figs. 8(c)–(f). The most localized state, Fig. 8(c), was the low-frequency gap state in Fig. 7(b). The eigenstate in Fig. 8(d) was located approximately at the original Bloch band edge, and the eigenstates in Figs. 8(e) and (f) were inside the band. The eigenstates in Figs. 8(c) and (d) were remeasured with a log amplifier, and linear fits to this data indicated localization lengths of $(2.2\pm 0.3)a$ and $(3.8\pm 0.3)a$, respectively; these agreed well with computer simulations. It should be noted that different eigenstates are localized at different sites in the system, and have different localization lengths. These factors would determine the transmission of the wave through the system (related to quantum electrical conductivity), and the wide variation in these factors is analogous to ''universal conductance fluctuations'' and transport ''fingerprints'' (Lee and Stone, 1985; Altshuler, Lee, and Webb, 1991).

B. Classical Anderson localization in higher dimensions

Guided by discussions in the preceding section, a scheme for observing classical Anderson localization in two or three dimensions would be to begin with an array of high-Q local oscillators with slightly different eigenvalues, and then weakly couple them together in a two- or three-dimensional pattern. With weak coupling, a periodic system would have narrow bands and mostly gaps; the introduction of sufficient disorder would lead to Anderson localized states.

A method for accomplishing this with acoustical waves is illustrated in Fig. 9. A number of aluminum plates (one of which is shown in Fig. 9) are machined on one side with hemispherical depressions, together with interconnecting semicylindrical channels. Each plate is machined the same way on the opposite side, and holes are drilled through connecting the bottoms of the hemi-

spheres. The plates are then stacked and sealed together, resulting in a three-dimensional array of spherical cavities connected with cylindrical necks. Acoustically this would be an array of coupled Helmholtz resonators; narrow necks would correspond to weak coupling. The system as described would be periodic, having identical Helmholtz resonators, and could be tested for Bloch wave behavior. For a disordered system, ''stuffing blocks'' of various sizes could be placed inside the spherical cavities, shifting the local Helmholtz resonance frequencies and introducing diagonal disorder.

A similar scheme could be imagined for microwaves, perhaps constructed with superconducting material to maintain high Q. One could also design a two-dimensional system on a printed circuit board with local capacitors and inductors, coupled with stripline waveguides. There are large numbers of possible systems of two-dimensional arrays of coupled mechanical or electromagnetic oscillators which one could construct. However, there is little point in actually using these classical systems for serious experimental research. The problem is that following the guidelines to readily observe Anderson localization leads to systems consisting of lumped elements connected by waveguides, which can be treated exactly in (linear) theory, and numerical computer calculations of eigenvalues and eigenfunctions could be carried out to high accuracy, far better than one could obtain experimentally. The fundamental physics governing the wave nature of the classical experiments is well established, so that if any significant deviations from the calculated results were observed in an experiment, the only valid conclusion would be that the experiment must be cleaned up. Properly designed experiments could be used for pedagogical purposes, student lab experiments, or lecture demonstrations. Classical experiments could also be used to study systems where the theoretical calculations are not so tractable, as for media not consisting of local oscillators (Weaver, 1990), for time-dependent potential fields or for the nonlinear Schrödinger equation. These last two possibilities are discussed in later sections.

In the literature one sometimes encounters the statement that it is difficult to observe classical Anderson localization. In light of the discussion above it would seem that this statement is quite untrue. However, this statement is sometimes made in regard to localization experiments which are motivated by the prospect of practical applications, such as optical waveguide multiplexers, etc., where constraints prevent the use of weakly coupled high-Q local oscillators. In this case, obtaining localization effects may be a formidable experimental challenge.

III. EFFECTS OF INELASTIC SCATTERING ON ANDERSON LOCALIZATION

The experiment described above was undertaken for pedagogical reasons, since Anderson localization in one dimension is guaranteed by Furstenberg's rigorous theorem. However, in the course of this experiment it was realized that it was possible to use the apparatus to address some serious questions in Anderson localization. The first question addressed involves the effects of inelastic scattering on Anderson localization.

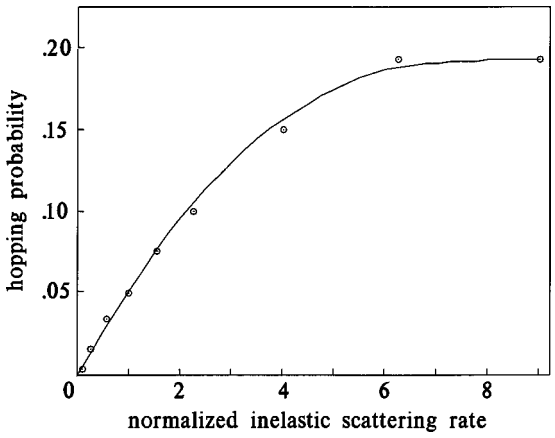

FIG. 10. Hopping probability as a function of strain amplitude, expressed as a normalized inelastic scattering rate (see He and Maynard, 1986).

If one considers an electron wave in a one-dimensional potential as being represented by the transverse wave in the wire-mass system, then an electron-phonon interaction may be simulated by modulating the longitudinal strain in the wire. That is, for low-frequency (essentially zero wave-vector) phonons, the electron-phonon interaction may be modeled by replacing the potential $V(r)$ in Eq. (2) by $V(r+r\epsilon\cos\Omega t)$ where $\epsilon\cos\Omega t$ is the strain field of a phonon of frequency Ω (Ziman, 1960). In the experiment the longitudinal strain is modulated directly with a second electromechanical actuator at the end of the wire, as shown in Fig. 4. By driving the longitudinal actuator with a synthesized ''thermal phonon'' spectrum, finite temperature effects could be simulated. However, in order to study an isolated inelastic scattering process in detail, only a single frequency Ω, providing the well-defined time-dependent potential $V(r+r\epsilon\cos\Omega t)$, is used.

For the inelastic scattering measurements one of the eigenstates in Figs. 8(c)–(f) was selected as an initial state $|i\rangle$, and another was chosen as a final state $|f\rangle$. The transverse actuator was driven at the initial state eigenfrequency ω_i, and the longitudinal actuator was driven at the frequency for resonant phonon-assisted hopping, $\Omega=|\omega_i-\omega_f|$. The response of the system, represented as a mixture $\alpha|i\rangle+\beta|f\rangle$, was then measured as a function of the amplitude of the longitudinal strain modulation amplitude ϵ. The steady-state response consisted of energy being transferred back and forth between the two states $|i\rangle$ and $|f\rangle$ at the frequency Ω. The time average of the mixture for a particular longitudinal strain amplitude is shown in Fig. 8(g). If the actuators were stopped, energy would be transferred to the final state with a hopping probability of $|\beta/\alpha|^2$. A plot of the measured hopping probability as a function of the longitudinal drive amplitude is presented in Fig. 10, where the initial and

final states were those of Figs. 8(d) and (e), respectively. Other pairs of states, cd, ce, cf, df, and ef, where the letters refer to Fig. 8, gave similar plots, but with widely varying vertical scales.

A significant conclusion of the inelastic experiment was that the large variations in the scale of hopping probability could not be wholly accounted for with the variations in the overlap of the amplitudes of the wave functions. At least in the case where the phonon wavelength is larger than the localization length, the phase as well as the amplitude overlap strongly influences the hopping rate. This is important for understanding the finite temperature behavior of electrons in disordered metal wires, and was a significant contribution from a classical analog system (He and Maynard, 1986).

IV. THE DISORDERED NONLINEAR SCHRÖDINGER EQUATION

As already discussed, there has been considerable research involving Anderson localization, with interest in mesoscopic electronic systems, in optical and acoustical systems, and in systems of practical interest, such as found in fiber optics, geophysical surveys, and noise control. Similarly, there has been a great deal of research and new insights into nonlinear physics, including the phenomena of solitons and chaos, and there are many systems for which an understanding of nonlinear effects is important. However, many systems of interest are both disordered and nonlinear, and the study of such systems is challenging. For systems which are both disordered and nonlinear, a fundamental question is: Does nonlinearity weaken or destroy Anderson localization? Despite the difficulties in treating this problem theoretically, there have been impressive achievements (Devillard and Souillard, 1986; Fröhlich *et al.*, 1986; Doucot and Rammal, 1987; Albanese *et al.*, 1988; Li *et al.*, 1988; Knapp *et al.*, 1989; Bourbonnais and Maynard, 1990; Kivshar *et al.*, 1990; Scharf *et al.*, 1992). Classical analogs of the nonlinear Schrödinger equation with a disordered potential field have been used to address unanswered questions as well as verify theoretical predictions.

One of the interesting aspects of the question concerning nonlinearity and Anderson localization is that the answer depends on how the question is posed, or how a system is studied. For example, one may study the wave mechanics of a one-dimensional system by exciting it at one end with a continuous wave $\cos(\omega t)$ and examining the transmission spectrum at an exit point $T(\omega)$. On the other hand, one may launch a pulse into the system and study the temporal response at the exit point $\psi(t)$. In a linear system the two results would be equivalent, simply related by a Fourier transform. However, this is no longer true for a nonlinear system, and different results may be obtained.

For continuous wave excitation of a one-dimensional (1D) nonlinear disordered system, theory predicts that eigenstates remain localized. Some of the theory papers (Fröhlich *et al.*, 1986; Albanese *et al.*, 1988; Knapp *et al.*, 1989) develop rigorous theorems, as for example, the paper by Frölich, Spencer, and Wayne (FSW) (Fröhlich *et al.*, 1986). This paper considers the existence of exponentially localized solutions of a Hamiltonian with a nonlinear term, and the result is that under general conditions Anderson localization is still present when there is nonlinearity. An interesting problem is the possibility of resonant tunneling resulting from the nonlinearity. In a linear disordered system, resonant tunneling is rendered unlikely by the low probability of having two resonant subsystems sufficiently close together to overcome the exponential decay of the wave function between the subsystems; the result is large resonance free regions in the spectrum, and the subsequent absence of diffusion. A gap in the FSW theory is whether or not there exist special conditions which result in resonant tunneling, enhanced by the nonlinearity, between localization sites. A classical analog system involving continuous waves has been used to address this question (McKenna *et al.*, 1992).

The theoretically predicted behavior for a pulse in a nonlinear disordered system is quite interesting (Li *et al.*, 1988; Kivshar *et al.*, 1990; Scharf *et al.*, 1992), and might be described with a simple picture as follows. One first considers a linear, 1D system of scatterers of length L, which may be analyzed by starting at one end and proceeding to the other end by multiplying two-by-two matrices (with elements for incident and reflected waves) at the position of each scatterer. For a disordered sequence of scatterers, one will have formed a product of random matrices, and by Furstenberg's theorem (Furstenberg, 1963), a sufficiently long system will have localized states and the transmission of a pulse will decay exponentially with the length of the system. An important point is that the behavior of a linear pulse, equivalent to a superposition of eigenstates, depends on satisfying conditions throughout the system. By contrast, a nonlinear pulse has extra degrees of freedom which may be adjusted so that conditions need be satisfied only locally, within a characteristic distance (e.g., the width of a soliton). In addition to the Anderson localization length, there is now a second, ''nonlinearity'' length. The consequences for a nonlinear pulse may be understood as illustrated by the lines in Fig. 11, which shows the log of the transmitted amplitude versus pulse propagation distance L (Kivshar *et al.*, 1990). If the nonlinearity of the pulse is weak so that the nonlinearity length is greater than the Anderson localization length, then the pulse transmission exponentially decays with L, as for a linear pulse (indicated by the dashed line in Fig. 11). If the nonlinearity of the pulse is strong, so that the nonlinearity length is much less than the Anderson localization length, then the effective extent of the disorder is insufficient to yield localization, and the pulse may show no exponential decay for large L (indicated by the dot-dashed line in Fig. 11). An interesting situation is when the nonlinearity length and the Anderson localization length are comparable. In this case theory predicts that the pulse will be transmitted for short L with moderate decay, but for larger L it will exponentially decay. This

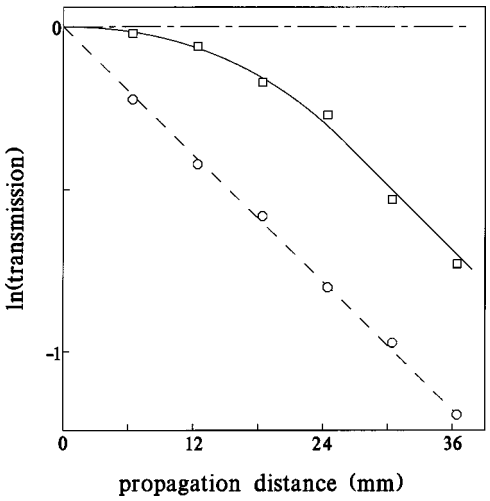

FIG. 11. Log of pulse transmission versus propagation distance. The dashed line is for weak nonlinearity, where the nonlinearity length is greater than the Anderson localization length. The dot-dashed line is for strong nonlinearity, where the nonlinearity length is less than the Anderson localization length. The interesting case, illustrated by the solid line, is when the two lengths are comparable (see Kivshar *et al.*, 1990). The symbols are data from the third-sound experiment.

case, illustrated by the solid line in Fig. 11, was verified with a classical analog experiment involving pulses (Hopkins *et al.*, 1996).

A. Continuous-wave excitation

For the study of continuous-wave excitation of a 1D nonlinear disordered system, the classical analog experiment is the same as that used to study Anderson localization and inelastic effects in the linear regime, i.e., the mass loaded steel wire. It should be noted that the nominal transverse wave speed c_0 in this system depends on the tension in the wire, $c_0=\sqrt{T_0/\mu}$, and for the experimental system, $c_0\simeq 400$ m/s. The masses were spaced with 2% disorder, which produced localization lengths on the order of $3a$ (He and Maynard, 1986). The method of making measurements was as follows: an amplitude for the drive actuator was selected, the receiver transducer was left in one position, the frequency of the drive was slowly swept, and the spectral response of the system was recorded. Using the spectral response, particular frequencies, corresponding to Anderson localized states at low amplitudes, could be selected, and the receiver transducer could be translated along the wire, recording the wave field for the selected frequency. The measurements were repeated for a sequence of increasing drive amplitudes, revealing the effects of the nonlinearity of the system.

The nature of the nonlinearity in this system is one of the important aspects of the experiment. To derive the nonlinear equation governing the system, one first considers how the experimental situation is established. One begins with an unstretched wire of length L_0, then applies the tension T_0 so that the wire stretches to a length $L=L_0+\Delta L$, and then adds the masses. The straight wire of length L is the equilibrium configuration for the system. For infinitesimal transverse displacements from equilibrium the equation of motion for the wire is

$$\mu\frac{\partial^2\Psi}{\partial t^2}-T_0\frac{\partial^2\Psi}{\partial x^2}=0, \tag{6}$$

where $\Psi(x,t)$ is the transverse displacement field of the wire. If the wire had a finite transverse displacement, then the arc length of the wire would be greater than L, and the tension in the wire would increase. Any local increase in tension in the wire would travel as a longitudinal sound wave in the wire. Because the speed of longitudinal sound in the steel wire is much greater than the speed of the transverse waves in the wire, any change in the tension due to a local transverse displacement produces a virtually instantaneous change in the overall tension of the wire. A good approximation for the net tension T in the wire simply involves the change in arc length for the entire wire:

$$T=T_0+\frac{T_0}{(\Delta L/L)}\frac{1}{L}\left[\int_0^L\sqrt{1+\left(\frac{\partial\Psi}{\partial x}\right)^2}\,dx-L\right], \tag{7}$$

where $T_0/(\Delta L/L)$ is an experimentally accessible expression for the Young's modulus of the wire. A more rigorous derivation of Eq. (7) may be found in Morse and Ingard (1968). Equation (7) may be expanded to first order in $(\partial\Psi/\partial x)^2$ and used to replace T_0 in Eq. (6) to yield the nonlinear equation of motion

$$\mu\frac{\partial^2\Psi}{\partial t^2}-T_0\left[1+\frac{1}{2\Delta L}\int_0^L\left(\frac{\partial\Psi}{\partial x}\right)^2dx\right]\frac{\partial^2\Psi}{\partial x^2}=0. \tag{8}$$

Because the nonlinear term involves an integral of the displacement field, the nonlinearity is nonlocal, and this increases the possibility of having nonlinear enhanced tunneling between two localization sites. That is, a large amplitude transverse displacement at one localization site will modulate the tension in the entire wire at twice the eigenstate frequency. This modulated tension may then parametrically excite a response at a distant localization site. The eigenfrequency (at low amplitude) of the distant site may even differ somewhat from that of the original site. The reason is that the finite amplitude displacement also increases the effective static tension of the wire, so that lines in the spectral response are bent toward higher frequencies, and may be bent over on top of one another (Morse and Ingard, 1968). In this case states with different frequencies at low amplitude may be excited concurrently at the same frequency at finite amplitude. The initial conditions of the experiment (as relevant to the FSW theory) are arbitrary, depending on the state of the system prior to adjusting the frequency of the drive.

With the possible nonlinear effects having been discussed, the actual experimental results can be presented. The simplest way to view the results is to examine the spectral response (amplitude at a fixed site as a function of frequency), measured at a distance of about four localization lengths from the drive actuator and normal-

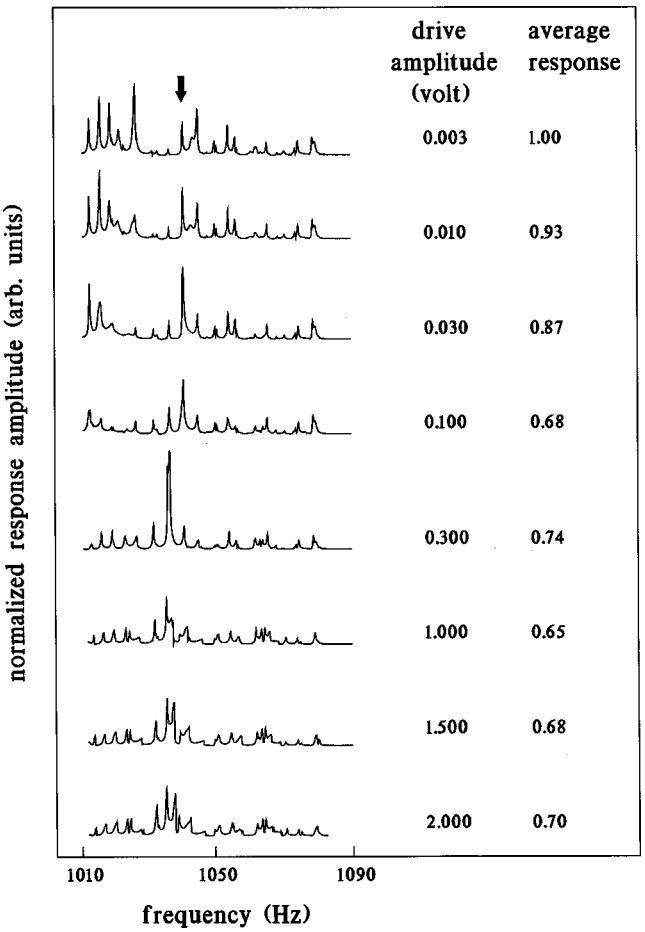

FIG. 12. Normalized spectral response for a sequence of drive amplitudes. The left-hand column of numbers displays the drive amplitude, expressed as the amplitude of the electrical signal applied to the drive actuator in volts. The right-hand column of numbers presents the "average response," defined as the integral of the normalized spectral response over the entire frequency band and normalized to the value at the lowest drive level (0.003 V). The arrow indicates a state whose normalized amplitude increases with drive amplitude, but the effect does not persist.

ized by dividing by the drive amplitude, for different drive amplitudes. If the system were strictly linear, then the normalized response would not change. If the Anderson localization is weakened by the nonlinearity, then as the drive amplitude is increased, the normalized response at the distant site should increase.

The experimental results are presented in Fig. 12, which shows a sequence of normalized spectral response plots for a sequence of increasing drive amplitudes. The drive amplitude, expressed as the amplitude of the electrical signal applied to the drive actuator in volts, is shown in the left column of numbers in Fig. 12. Below the lowest amplitude in Fig. 12, the spectral response shows little variation, but in the sequence of increasing drive amplitudes shown, the spectral response shows some change. For some of the peaks in the spectrum, for example the one indicated by the arrow in Fig. 12, the normalized response increases with increasing drive amplitude, suggesting that there might be some weakening

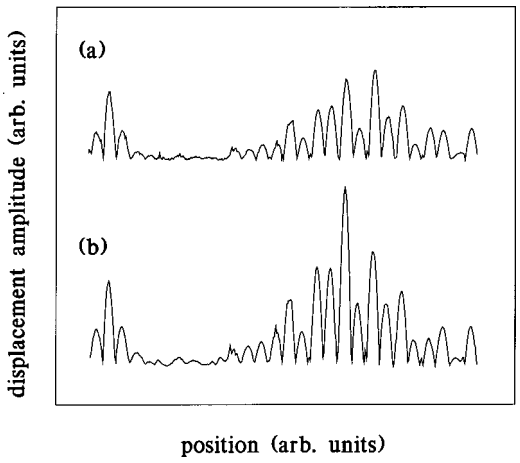

FIG. 13. The wave amplitude, normalized with the drive amplitude, versus position, with the drive actuator to the left of the figure. (a) The wave field for a drive amplitude of 0.01 V. (b) The wave field for a drive amplitude of 0.50 V.

of the Anderson localization. However, this effect does not seem to persist to the highest drive levels. Furthermore, an examination of the wave fields for the peaks which increase indicates that the effect is due to the growth in amplitude of sections of wire between a few masses only. Figure 13 shows an example of one such wave field whose peak increased with increasing drive amplitude. Figure 13(a) is the wave field (wave amplitude, normalized with the drive amplitude, versus position, with the drive to the left in the figure) for a drive of 0.01 V, and Fig. 13(b) is the wave field for a drive of 0.50 V. While the normalized amplitudes of a few sections have increased, the Anderson localization has not changed significantly. It should be noted that for the wave field in Fig. 13, and in all of the measured wave fields, there was no significant harmonic generation observable.

None of the wave fields at any frequency which was measured showed any significant reduction of Anderson localization, in accord with the FSW theory. Furthermore, an examination of wave fields most likely to show nonlinear enhanced tunneling (i.e., states at nearly the same frequency localized at different sites) gave no evidence of enhanced tunneling. The highest drive amplitude in the measurements corresponded to a nonlinear shift in the eigenfrequencies by as much as 15% of the bandwidth (quite large by acoustic standards). Proceeding to higher drive amplitude was prevented by the onset of strong chaos in the system; because the Anderson localization concentrates the wave energy in a limited region, the state may act like a simple oscillator which might easily go chaotic.

Returning to Fig. 12, it can be seen that most of the normalized response seems to decrease slightly with increasing drive level, indicating stronger localization. A quantitative measure of this effect may be found with an "average response," defined as the integral of the normalized spectral response over the entire frequency band. The results for each drive level, normalized to the value at the lowest drive level in Fig. 12, are presented in

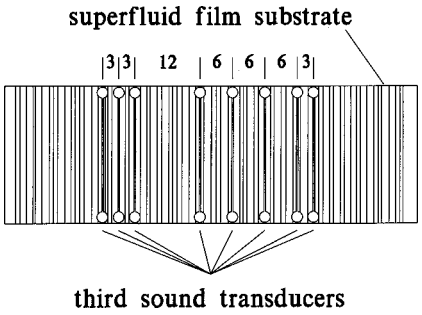

FIG. 14. Top view of the superfluid helium film substrate, showing the configuration of third-sound transducers and the disordered sequence of scatterers. The distances between adjacent transducers, in millimeters, are indicated by the numbers.

the right-hand column of numbers in Fig. 12. The decrease in the average response of about 30% with increasing drive amplitude suggests that the Anderson localization is slightly enhanced by the nonlinearity. One might imagine that the nonlinearity causes an Anderson localized state not to parametrically excite a distant site, but rather to "dig a deeper hole" for itself.

B. Pulse propagation

The case of nonlinear pulse propagation was studied with another classical analog experiment. In this case, surface waves on a fluid were used because such waves are intrinsically nonlinear. That is, the speed of the surface wave depends on depth, but the depth is modified by the presence of a finite amplitude surface wave; having the wave speed depend on the wave field leads naturally to a nonlinear wave equation. An important consideration is that the system have minimum damping, since long-range phase coherence is required to have Anderson localization. Because of this, surface waves on thin films of superfluid helium adsorbed on a substrate were used; such waves are referred to as third sound (Atkins and Rudnick, 1970). In this system the normal fluid component of the helium is locked to the substrate by its viscosity, and only the zero-viscosity superfluid component moves, resulting in relatively little damping of the surface waves. The nonlinear nature of third sound may be summarized as follows: When third-sound pulses are generated with sufficient amplitude, the initial part of the pulse saturates (probably because the motion of the superfluid comprising the pulse exceeds a critical velocity). Subsequent increases in the energy delivered by the drive transducer causes a second pulse to appear and move away from the saturated pulse. This pulse is observed to be nonlinear in nature not only because it exists due to finite amplitudes and is unexplained by the linear theory, but also because its velocity of propagation depends on amplitude (McKenna *et al.*, 1990).

An illustration of the experimental configuration is shown in Fig. 14, which is a top view of the superfluid film substrate, consisting of a $25\times75\times1$-mm glass plate. The substrate is held in a container at a temperature of 1 K, and helium vapor is admitted into the container until a superfluid film forms on the substrate. The third-sound transducers are strips of superconducting aluminum film deposited across the width of the substrate, with pads for electrical connection at each end. When used as third-sound generators, a strip is activated with a pulse of current which drives the aluminum film normal, and the resulting Joule heating launches the third-sound pulse; the strips act as line sources, so that a plane wavefront pulse propagates in each direction down the length of the glass substrate. By monitoring the current, voltage, and time duration of the electrical pulse sent to the transducer, the energy used to generate the third-sound pulse is calculated. As receivers, the aluminum film strips act as conventional superconducting bolometers.

The 1D sequence of scatterers is formed by cutting grooves across the width of the glass substrate (parallel to the transducers, as shown in Fig. 14) with a diamond wire saw. The scatterers have an average spacing of 1 mm, and are given a random displacement within ±0.5 mm of the average spacing. Using the actual disorder and the magnitude of the reflection coefficient, a computer simulation indicated that the Anderson localization length was on the order of 18 ± 2 mm.

An important aspect of Anderson localization is that different realizations of disorder, although the same statistically, give widely fluctuating results. Thus in order to obtain meaningful conclusions, it is helpful to ensemble average. For this purpose different pairs of transducers were used as generators and receivers, and results from pairs which had the same nominal separation were averaged. The relative separations of the transducers, in millimeters, are indicated by the numbers in Fig. 14; the nominal separations for the various pairs used in the experiment range from 6 to 36 mm, in steps of 6 mm, as indicated by the abscissa values of the data points in Fig. 11.

For a measurement sequence in the experiment, one transducer was selected as a third-sound generator, and a second selected as receiver. Pulses were launched with generator energies ranging from 25 nJ, well into the linear regime, to 1200 nJ, well into the nonlinear regime. For each energy level, received wave forms (transducer signal as a function of time) were sample averaged and recorded. The ensemble averaged results for pulse amplitude as a function of distance, for different generator amplitudes, are presented as the symbols in Fig. 11. The circles are for a nominal generator energy of 275 nJ; at this energy a nonlinear signal is readily observed, but its transmission exponentially decays, so that the theory would indicate that at this energy the nonlinearity length is greater than the Anderson localization length. The squares in Fig. 11 are for a nominal generator energy of 975 nJ. In this case the decay in the transmission is significantly smaller for the shorter propagation distances, with exponential decay not occurring until after about one Anderson localization length. This is in excellent qualitative agreement with the theoretical prediction, indicated by the solid line in Fig. 11. It should be noted that the third sound in the linear regime behaved as

expected, with a measured Anderson localization length of 22 ± 2 mm, in reasonable agreement with the computer simulation.

Measurements for nonlinear pulse propagation in a periodic array of scatterers (McKenna *et al.*, 1994) have also been made. In this case it was found that for lower generator energies, the nonlinear signal showed structure resulting from coherent interference in the periodic array, and a Fourier transform of the signal showed band structure. For high generator energies, the interference structure disappeared (along with the band structure). The interpretation is that at the high amplitudes, the nonlinearity length is sufficiently short so that the wave does not sample enough of the periodic array to produce observable structure. The conclusion is that the concept of a nonlinearity length, which decreases with the amplitude of a pulse, is valid for pulses in disordered as well as periodic media, and the classical experiment verified theoretical predictions.

V. MESOSCOPIC NORMAL ELECTRON PERSISTENT CURRENTS

One of the most interesting puzzles in mesoscopic physics has been the discrepancy between the theoretically predicted and experimentally measured amplitudes of persistent currents in mesoscopic normal metal rings (Levy *et al.*, 1990; Chandrasekhar *et al.*, 1991). An acoustical analog system was used to address this puzzle, and the experiment indicated that one must consider the effects of wave attenuation, which is the analog of residual inelastic scattering in the normal electron system, and the nature of the excitation field. While the acoustical system is not a complete analog of the normal electron persistent current experiment (e.g., there is no precise analog of many electron effects), the results do suggest a wave mechanical approach to the nature of the mesoscopic experiment which can account for the observed discrepancy. An interesting feature of the experiment is the acoustical analog of a magnetic field.

The normal electron persistent current experiment, such as that of R. Webb *et al.* (Chandrasekhar *et al.*, 1991), involves a normal-metal ring surrounded by a drive loop and squid pickup loop. The pickup loop monitors the current in the ring, through its mutual inductance, as the magnetic flux Φ in the system is changed with the drive loop. The current in the ring is found to oscillate with a period of $\Phi_0=h/e$, the normal electron flux quantum, as predicted by theory. However, the magnitude of the current oscillations exceed the theoretically predicted value by more than an order of magnitude.

For an initial model of the ring, consider an ideal circular waveguide, with circumference L and eigenstates $\psi\propto\exp(\pm i2\pi x/\lambda)$, where λ is the wavelength and x is a coordinate which follows the waveguide. A current associated with the eigenstate is given by

$$I=ne\frac{i\hbar}{2m}(\psi^*\nabla\psi-\psi\nabla\psi^*)=neh/m\lambda, \tag{9}$$

where m and e are the electron mass and charge, and n is the number of electrons per unit length in the ring (spin is ignored). The quantization condition is that an integral number of wavelengths must fit in the circumference L, so that $L=N\lambda$, and $I=N(neh/mL)$. Since N is an integer, I is quantized in units of

$$\Delta I=\frac{neh}{mL}=\frac{ev_F}{L}, \tag{10}$$

where $v_F=nh/m$ is the Fermi velocity. As will be shown next, current oscillations of magnitude ΔI in the ideal ring correspond to changes in magnetic flux through the ring of magnitude Φ_0.

An actual normal-metal ring would not be a perfect waveguide, because it will contain defects which elastically scatter the wave. We consider a large section of the waveguide as containing all of the defects. At one end of the scattering section we write the eigenfunction as a combination of two linearly independent solutions:

$$\psi=Ae^{i2\pi\Phi/\Phi_0}e^{i2\pi x/\lambda}+Be^{i2\pi\Phi/\Phi_0}e^{-i2\pi x/\lambda}. \tag{11}$$

The factor $\exp(i2\pi\Phi/\Phi_0)$ arises from the vector potential term in the Schrödinger equation. For the other end of the scattering section we assume a similar form for the eigenfunction, but use coefficients A' and B'. From general scattering theory we have

$$A=(1/T)A'+(R/T)^*B', \tag{12}$$

$$B=(R/T)A'+(1/T)^*B', \tag{13}$$

where R and T are the complex reflection and transmission coefficients for the scattering section. From conservation of flux, $|R|^2+|T|^2=1$. We require periodic boundary conditions, so that ψ and its derivative must match at $x=0$ and $x=L$. With Eqs. (12) and (13), we now have four equations for A, B, A', and B'. For nonzero solutions, the determinant of the coefficients must vanish, yielding the eigenvalue condition

$$2\pi L/\lambda=N2\pi=\tan^{-1}[\mathrm{Im}(T)/\mathrm{Re}(T)] \pm\cos^{-1}[|T|\cos(2\pi\Phi/\Phi_0)]. \tag{14}$$

Note that if there were no scatterers, then $T=1$, and changes of one quantum in the eigenvalue (or changes of $\Delta I=ev_F/L$) correspond to changes of Φ_0 in Φ. More significantly, if there are scatterers, then $|T|<1$, and while the period of the oscillations in Φ remains Φ_0, the magnitude of the oscillations in ΔI is reduced. If one assumes that $|T|^2\simeq L_e/L\leqslant1$, where L_e is the mean free path for the elastic scattering, then one has

$$\Delta I\simeq\frac{ev_F}{L}\frac{L_e}{L}. \tag{15}$$

A simple way of formulating Eq. (15) is to note that as a consequence of the elastic scattering, the electron must follow a tortuous path around the ring, so that the effective length of the waveguide is $L'\simeq L(L/L_e)$. Equation (15) becomes

$$\Delta I=\frac{ev_F}{L'}=\frac{ev_F(L/L')}{L}. \tag{16}$$

In the normal electron persistent current experiments, L/L' is determined with a transport (quantum conductivity) measurement. When this value (typically 0.01–0.1) is used in Eq. (16), one obtains values of ΔI which are more than an order of magnitude smaller than the values of ΔI found in the actual experimental persistent current measurement.

The current quantization as discussed above arises from a difference between eigenvalues, and one must consider whether or not a particular experimental probe is sensitive to all of the eigenstates and eigenvalues. If a system having no inelastic scattering (or no wave attenuation) is subjected to an excitation field, then all states appear as "delta function" contributions to the response of the system, unless the excitation field is exactly orthogonal to a particular eigenfunction. If one had an ideal lossless system with a realistic excitation field, then it would be very difficult to have the excitation not couple to all of the eigenstates. However, if there is significant wave attenuation in the system, then the "delta function" response no longer occurs, and the nature of the excitation field becomes a more serious concern. The application of this notion to the system of general elastic scatterers described above and the theory of quantum measurement is beyond the scope of this paper. However, one could test the consequences of this notion with an acoustical analog system.

The difference between Eq. (10) and Eq. (16), i.e., replacing v_F by $v_F(L/L')$, is analogous to the "acoustic scattering correction" used for long-wavelength sound undergoing multiple scattering in a disordered array of scatterers. A model used to study the acoustic scattering correction can now be used to gain insight into the effects of the excitation field.

In the acoustic scattering model, one first imagines a "black box" of length L, containing a straight waveguide, also of length L. One sends in a wave, $\exp(i\omega x/v_0)\exp(-i\omega t)$, and measures the total phase shift θ_0 across the box. Since $\theta_0=\omega L/v_0$, one could determine the speed of the wave as $v_0=\omega L/\theta_0$. One next considers a box of length L containing a meandering waveguide (with a "square wave" shape) with a total length $L'>L$. The phase shift across this box would be $\theta=\omega L'/v_0=\theta_0(L'/L)$, but not knowing what was inside the box, one would calculate a wave speed $v=\omega L/\theta=v_0(L/L')$. This is analogous to the effective velocity $v_F(L/L')$ in Eq. (16).

For the normal electron persistent current experiment, one imagines the "square wave" waveguide (of length L') bent into a ring of circumference L, as shown in Fig. 15. If a drive transducer (a point source) were placed at one point on the waveguide, and a receiver transducer were placed diametrically opposite, then a wave could be sent around the ring, as shown in Fig. 15(a). The phase advance at the receiver transducer could be used to determine the wave velocity, and one would calculate a velocity $v=v_0(L/L')$, as before. However, such a measurement, with a "point source" excitation field, would correspond to a transport measurement; an important point is that a persistent current measurement is fundamentally different from a transport measurement.

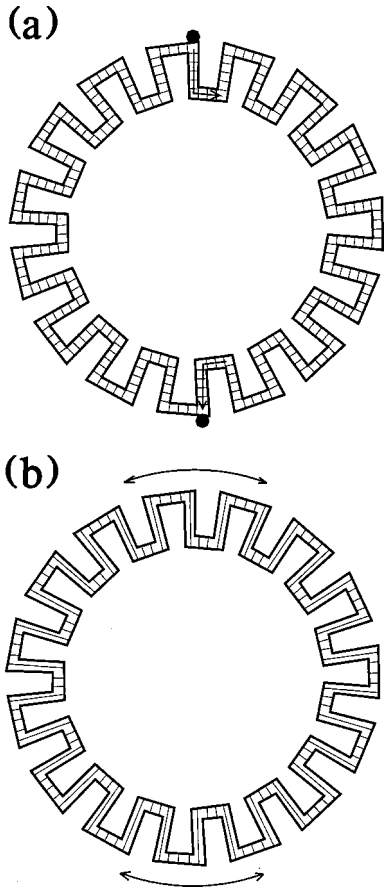

FIG. 15. Different methods of exciting a circular, meandering waveguide. (a) A simple source and detector at diametrically opposite points are analogous to a transport measurement and involve the length L'. (b) An ac azimuthal excitation field is analogous to a persistent current measurement and involves the length (circumference) L.

In the persistent current measurement, the state of the system is probed with an ac axial magnetic field. The ac axial magnetic field produces an excitation field at the ring which is uniform and purely azimuthal; there is no radial component. In the acoustical system, the analog of the axial magnetic field would be a rotation of the acoustic fluid; the Doppler shift of the sound introduces a shift in the phase of the waves in analogy with the phase shift in the electron Schrödinger wave produced by the magnetic field (flux) as indicated in Eq. (11). The analog of the ac axial magnetic field would be an oscillation of the "square wave" waveguide about its axis, producing a purely azimuthal excitation field. The results of this type of excitation of the waveguide are quite different from those of the point source, as can be seen in Fig. 15(b). The axial oscillation would sustain an advance of the phase along the azimuthal parts of the waveguide, but not along the radial parts. The fluid in the radial parts of the waveguide would be driven back and forth between the sides of the waveguide, corresponding to a waveguide mode which has infinite phase

velocity along its length; i.e., there is no coupling to a phase advance along this part of the waveguide. The result is that the excitation field matches modes where the phase advance around the waveguide involves L rather than L', and the velocity determined from the phase would be v_0 rather than $v_0(L/L')$. If only these modes were involved in the persistent current experiment, the correct expression for ΔI would be ev_F/L, and this would give good agreement with the experimental results, removing the discrepancy.

A further example of the importance of the excitation field, with reference to the analogy between an acoustical system and the normal electron persistent current experiment, may be elaborated as follows. The response of a linear system may be written as a sum over normal modes, with each term having a numerator and a denominator. The denominator involves the difference between the driving frequency and the eigenfrequency of the normal mode, with an attenuation term which prevents the denominator from vanishing. The numerator involves an inner product between the driving excitation field and the normal-mode eigenfunction. In a transport measurement, the excitation field is a point (or slightly extended) source, so that the numerator has the same nominal value for all the (normalized) normal modes, and the response of the system has resonances when the denominator is minimized at the eigenfrequencies. For the analog of a persistent current measurement, imagine a one-dimensional acoustic waveguide with point scatterers; a flow of the fluid giving a Doppler shift of the sound wave provides the analog of the vector potential field. Between the point scatterers, the wave field may be written as a traveling wave in one direction, Doppler shifted up, and a traveling wave in the opposite direction, Doppler shifted down. Now imagine that the walls of the waveguide are lined with drive transducers whose phase may be independently controlled. These transducers may be phased so as to follow a traveling wave progressing, and Doppler shifted, in one direction only. The response of the system in this case will be dominated not by minima in the denominator, but instead by maxima in the numerator. If the fluid flow is increased so that the Doppler shift is increased, then the change in frequency of the drive required to follow the maximum in the response will be determined by the full Doppler shift, and will be unaffected by the effect of the scatterers. The effects of the change in the natural frequencies resulting from the change in the Doppler shift [rendered small by the scatterers as in Eq. (14)] in the denominator will be of less importance. In effect, the phased driving excitation projects out the unreflected part of the wave field.

Returning to the meandering waveguide model, it should be noted that in the absence of attenuation, the presence of phase-advancing waves in the azimuthal parts will excite some phase-advancing waves in the radial parts. However, if there is wave attenuation, the azimuthal excitation will favor modes with a purely azimuthal phase advance. The degree to which these modes

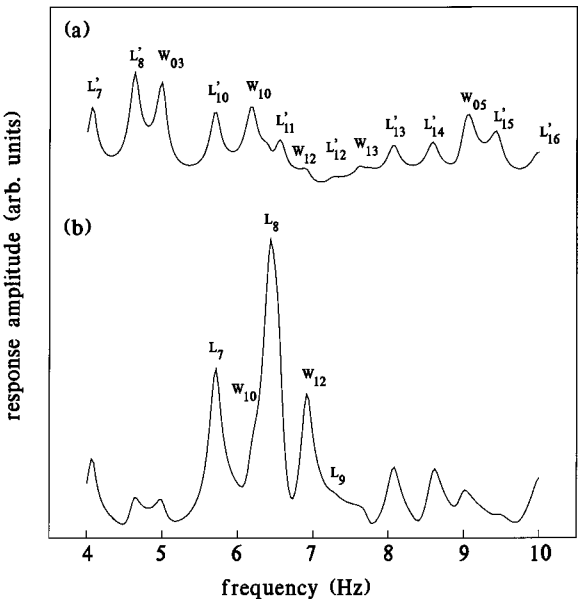

FIG. 16. Response spectra of an "L" shaped waveguide (the simplest element of a "square wave" meandering waveguide) for two different types of excitation. (a) Simple source excitation, showing nominal excitation of all modes. (b) Uniform one-dimensional excitation of the entire waveguide, showing preferential excitation of modes involving only the length L.

are favored is a difficult problem in waveguide theory. An acoustical analog experiment is used to gain insight into this problem.

The experiment involves a waveguide with the shape of an "L," which is the simplest element of a "square wave" waveguide. One end of the "L" has a receiver transducer, and the modes of the waveguide are excited in two different ways. One method of excitation uses a point source at the end of the waveguide opposite the receiver, which should excite modes which correspond to fitting an integral number of half wavelengths within the total length of the "L" waveguide (with a length L'). The second method of excitation is to drive the entire waveguide back and forth with a motion parallel to one arm of the "L" (with a length L). The second method should favor those modes which correspond to fitting an integral number of half wavelengths along the parallel arm of the "L," and which have no phase shift along the perpendicular arm of the "L." The results of the experiment are shown in Fig. 16; Fig. 16(a) shows the response as a function of drive frequency for the point source excitation, and Fig. 16(b) shows the results for the uniform one-dimensional excitation. The peaks in the spectra are labeled with an L or L' with a subscript indicating the number of half wavelengths which fit into the length L or L' respectively; the label W indicates waveguide modes of the perpendicular arm of the "L," with the first subscript indicating the number of half wavelengths across the waveguide, and the second subscript indicating the number of half wavelengths along the waveguide. The presence of the enhanced peaks in Fig. 16(b) confirm the predictions; the uniform one-dimensional drive does favor the modes with no

phase advance along the perpendicular arm of the waveguide. The effect may be greatly enhanced with a waveguide consisting of many of the ''L''-shaped elements. This classical analog experiment explains why electrons ''take the shortest path'' in going around a mesoscopic disordered metal ring.

VI. TUNING-UP A QUASICRYSTAL

Since the discovery of aluminum alloys with long-range fivefold rotational (quasicrystalline) symmetry by Shechtman *et al.* (1984), there has been great interest in this fascinating symmetry (Mermin, 1980; Levine and Steinhardt, 1986; Socolar and Steinhardt, 1986). A fundamental question is: given a Schrödinger wave equation with a quasicrystalline potential field, how is the quasicrystalline symmetry manifest in the eigenvalue spectrum and the eigenfunctions? For one-dimensional (1D) quasicrystalline systems, rigorous theorems (Simon, 1982; Kohmoto *et al.*, 1983; Ostlund *et al.*, 1984; Kohmoto *et al.*, 1986; Lu *et al.*, 1986; Luck and Petritis, 1986; Niu and Nori, 1986; Kohmoto *et al.*, 1987; Gumbs and Ali, 1988; Luban *et al.*, 1988; Onoda *et al.*, 1988) have been derived which answer such questions; however, in two and three dimensions there are as yet no accepted theorems. A two-dimensional acoustical analog experiment provided clear results (He and Maynard, 1989).

Determining the effects of quasicrystalline symmetry theoretically poses a challenging problem; for periodic potentials one may use Bloch's theorem and perform precise calculations, and for random systems one may use statistical techniques to determine useful quantities. However, quasicrystalline systems are neither periodic nor random, and with the exception of 1D systems there is currently no accepted ''quasi-Bloch's'' theorem for predicting the consequences of quasicrystalline symmetry. For 1D quasicrystalline systems, general theories have been reviewed by Simon (1982), and renormalization-group, dynamic mapping, and numerical techniques have been applied (Kohmoto *et al.*, 1983; Ostlund *et al.*, 1983, 1984; Kohmoto *et al.*, 1986; Lu *et al.*, 1986; Luck and Petritis, 1986; Niu and Nori, 1986; Kohmoto *et al.*, 1987; Gumbs and Ali, 1988; Luban *et al.*, 1988). Some special properties of 1D quasicrystalline systems are (i) the eigenvalue spectrum is a Cantor set (Lauwerier, 1991), (ii) there may exist a mobility edge and a metal-insulator transition, (iii) the eigenfunctions may be extended, localized, or critical. One-dimensional quasicrystalline systems have received some experimental attention (Merlin *et al.*, 1985).

By contrast the consequences of quasicrystalline symmetry in two and three dimensions have been less well verified; the transfer matrix method and the renormalization-group approach seem to be inapplicable. There are some known theorems dealing with structure (Penrose, 1974; Gardner, 1977), such as those involving inflation (deflation) rules and Conway's theorem, which states that a given local pattern of some diameter will be repeated within a distance of two diameters, and most probably within one diameter. In the absence of a quasi-Bloch theorem, progress in understanding the consequences of 2D quasicrystalline (Penrose tile) symmetry (Penrose, 1974; Gardner, 1977) has relied mostly on numerical calculations, but the models employed neglected aspects of the wave nature of the problem. There have been a few exact eigenfunctions discovered for 2D quasicrystalline systems (Sutherland, 1986; Arai *et al.*, 1988), but these only apply to certain eigenvalues or special Hamiltonians.

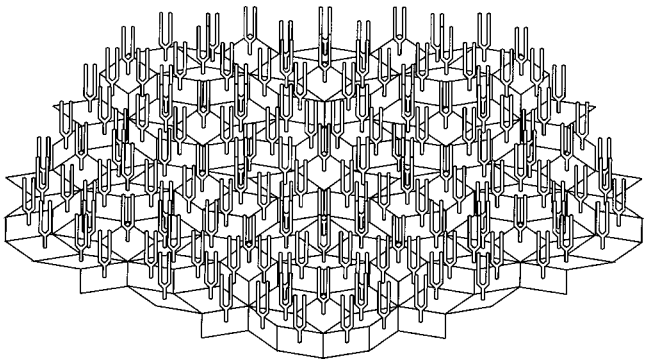

FIG. 17. A schematic drawing of a tuning fork quasicrystal. The tuning forks are mounted at the center of the rhombuses in the Penrose tile, with the two tines oriented in line with the shorter diagonal (for the sake of drafting simplicity, the tuning forks are not drawn with the correct orientation). For the nearest-neighbor coupling, arcs of steel wire (not shown) are spot welded from one tine of a tuning fork to that of a nearest neighbor.

As discussed earlier, the success of a classical analog experiment is enhanced by using high-Q local oscillators, coupled so as to model the appropriate symmetry. For the quasicrystal experiment, ordinary commercial tuning forks (440 Hz) were used. These have the advantage that they can be mounted by the stem and still maintain a high-Q oscillation. The tuning forks are epoxied in a 2D quasicrystalline pattern into a heavy aluminum plate; the pattern is a standard Penrose tile formed with two rhombuses (fat and skinny) having areas in the ratio of the Golden mean, $(\sqrt{5}+1)/2$. An illustration of the tuning fork quasicrystal is shown in Fig. 17. The tuning forks are mounted at the centers of the rhombuses, with the two tines oriented in line with the shorter diagonal (it should be noted that for the sake of simplicity in drafting Fig. 17, the tuning forks are not drawn with the correct orientation). For the nearest-neighbor coupling, arcs of 1-mm-diameter steel wire are spot welded from one tine of a tuning fork to that of a nearest neighbor. Other coupling schemes were tested and found to be either too weak, too lossy, or had too low a coupling wave velocity. Using the four sides of each rhombus, four nearest-neighbors are identified, and each tine of a tuning fork is coupled to the two nearest tines of the adjacent tuning forks. With this coupling pattern each local oscillator has four nearest neighbors, but the nearest-neighbor length varies in a quasicrystalline pattern. From a separate measurement of the fundamental resonance in an isolated arc of the coupling

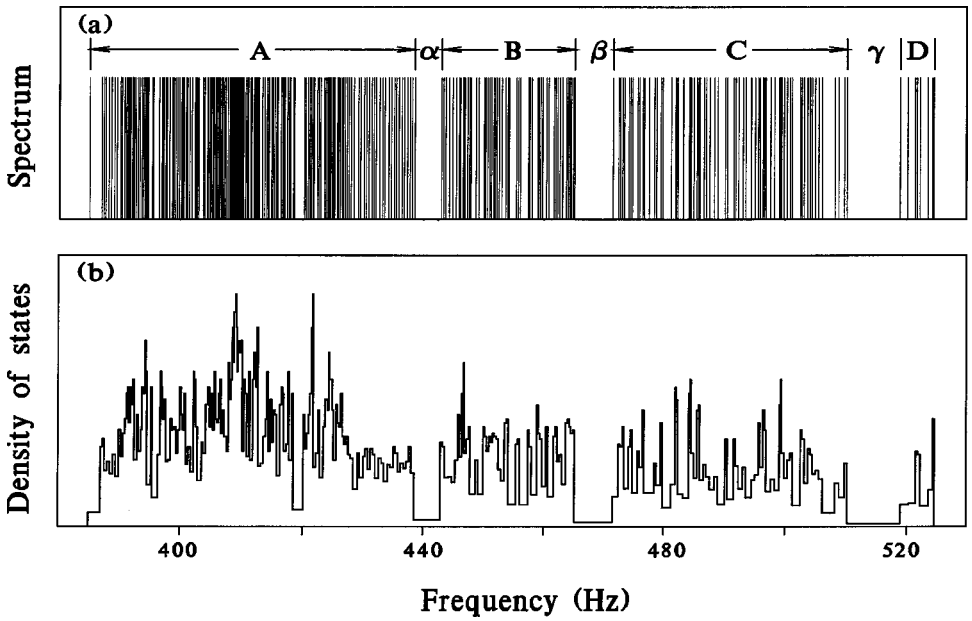

FIG. 18. The eigenvalue spectrum and density of states for the tuning fork quasicrystal. (a) The eigenvalue spectrum, determined as a composite of the resonant spectra from 20 different positions in the Penrose pattern, showing gaps and bands whose widths are in the ratio of the Golden Mean. (b) The density of states, as the inverse of the difference in frequency for neighboring eigenvalues.

wire, the nominal wavelength in the coupling wire system at 440 Hz was determined to be ~20 cm, or approximately 3–5 nearest-neighbor lengths. With a wavelength of this size, it is possible for the coupling wire system to interact with the quasicrystalline pattern in interesting ways and produce structure in the eigenvalue spectrum.

In order to drive the oscillations of the coupled tuning fork system, an electromagnet is positioned near one tine of the array, and an ac current is passed through the electromagnet. The response of the system is monitored with four electrodynamic transducers (electric guitar pickups) positioned next to random tines in the array. By sweeping the frequency of the drive electromagnet, the resonant response of the system is detected with the pickup transducers; the resonant frequencies, in bands near 440 Hz, correspond to the eigenvalues of the quasicrystalline system. The eigenvalue spectrum, determined as a composite of the resonant spectra from 20 different positions in the Penrose pattern, is presented in Fig. 18(a). This spectrum shows gaps and bands whose widths are in the ratio of the Golden Mean, $\tau=(\sqrt{5}+1)/2$. Referring to Fig. 18(a), $\beta/\alpha=\tau$, $\gamma/\beta=\tau$, $C/B=\tau$, $A/B=\tau^2$, $B/D=\tau^3$, and other ratios of combinations of these are powers of τ, with an average deviation of $\pm 5\%$. The density of states, determined as the inverse of the difference in frequency for neighboring eigenvalues, is shown in Fig. 18(b). This was not observed in numerical simulations, because the wave nature of the problem was not included in the models, and for two (and three) dimensions there are no theoretical predictions; thus the classical analog experiment provided a significant advance in the understanding of quasicrystalline symmetry.

VII. SUMMARY

Many interesting and important problems in condensed-matter physics involve quantum mechanics and the Schrödinger equation, which is a wave equation. It is possible to design macroscopic experiments with systems governed by a classical wave equation which accurately model salient features of quantum-mechanical systems. Having a "megascopic" scale, such experiments permit measurements of features and tests of phenomena which are virtually inaccessible on the microscopic, quantum scale. Furthermore, classical analog experiments may include time-dependent and nonlinear interactions, which are difficult to treat with analytical theory or numerical simulation. Using simple acoustic systems, significant research results have been obtained for Anderson localization, the effect of a time-dependent potential on localized states and phonon assisted hopping, the behavior of nonlinear pulses and continuous waves in a disordered system, an explanation of a discrepancy in a normal electron persistent current experiment, and the consequences of quasicrystalline symmetry in two dimensions. Insights provided by such analog experiments go a long way in helping to understand condensed-matter problems.

ACKNOWLEDGMENTS

This research was supported by NSF grants DMR 8304371, 8701682, 9000549, 9306791, and 9801844, and the Office of Naval Research.

REFERENCES

Albanese, C., J. Fröhlich, and T. Spencer, 1988, Commun. Math. Phys. **119**, 677.
Altshuler, B. L., P. A. Lee, and R. A. Webb, 1991, *Mesoscopic Phenomena in Solids* (North-Holland, Amsterdam).
Anderson, P. W., 1958, Phys. Rev. **109**, 1492.
Anderson, P. W., 1978, Rev. Mod. Phys. **50**, 191.
Arai, M., T. Tokihiro, T. Fujiwara, and M. Kohmoto, 1988, Phys. Rev. B **38**, 1621.

Atkins, K. R., and I. Rudnick, 1970, in *Progress in Low Temperature Physics*, edited by C. J. Gorter (North-Holland, Amsterdam), p. 37.
Bloch, F., 1928, Z. Phys. **52**, 555.
Bourbonnais, R., and R. Maynard, 1990, Phys. Rev. Lett. **64**, 1397.
Chandrasekhar, V., R. A. Webb, M. J. Brady, W. J. Gallagher, and A. Kleinasser, 1991, Phys. Rev. Lett. **67**, 3578.
Devillard, P., and B. Souillard, 1986, J. Stat. Phys. **43**, 423.
Doucot, B., and R. Rammal, 1987, Europhys. Lett. **3**, 969.
Floquet, G., 1883, Ann. Sci. Ecole Norm. Sup. **12**, 47.
Fröhlich, J., T. Spencer, and C. E. Wayne, 1986, J. Stat. Phys. **42**, 247.
Furstenberg, H., 1963, Trans. A. Math. Soc. **108**, 337.
Gardner, M., 1977, Sci. Am. **236**, 110.
Gumbs, G., and M. K. Ali, 1988, Phys. Rev. Lett. **60**, 1081.
He, S., and J. D. Maynard, 1986, Phys. Rev. Lett. **57**, 3171.
He, S., and J. D. Maynard, 1989, Phys. Rev. Lett. **62**, 1888.
Hopkins, V. A., J. Keat, G. D. Meegan, T. Zhang, and J. D. Maynard, 1996, Phys. Rev. Lett. **76**, 1102.
Ishii, K., 1973, Suppl. Prog. Theor. Phys. **53**, 77.
Kittel, C., 1996, *Introduction to Solid State Physics* (John Wiley & Sons, New York), Appendix D.
Kivshar, Yu. S., S. A. Gredeskul, A. Sanchez, and L. Vazquez, 1990, Phys. Rev. Lett. **64**, 1693.
Knapp, R., G. Papanicolaou, and B. White, 1989, in *Disorder and Nonlinearity*, edited by A. R. Bishop, D. K. Campbell, and S. Pnevmatikos (Springer-Verlag, Berlin).
Kohmoto, M., and J. R. Banavar, 1986, Phys. Rev. B **34**, 563.
Kohmoto, M., L. P. Kadanoff, and C. Tang, 1983, Phys. Rev. Lett. **50**, 1870.
Kohmoto, M., B. Sutherland, and C. Tang, 1987, Phys. Rev. B **35**, 1020.
Lauwerier, H., 1991, *Fractals: Endlessly Repeated Geometric Figures* (Princeton Press, Princeton, NJ), p. 15.
Lee, P. A., and T. V. Ramakrishnan, 1985, Rev. Mod. Phys. **57**, 287.
Lee, P. A., and A. D. Stone, 1985, Phys. Rev. Lett. **55**, 1622.
Levine, D., and P. J. Steinhardt, 1986, Phys. Rev. B **34**, 596.
Levy, L. P., G. Dolan, J. Dunsmuir, and H. Bouchiat, 1990, Phys. Rev. Lett. **64**, 2074.
Li, Q., C. M. Soukoulis, St. Pnevmatikos, and E. N. Economou, 1988, Phys. Rev. B **38**, 11888.
Lifshits, I. M., 1938, Zh. Eksp. Teor. Fiz. **9**, 959.
Lifshits, I. M., 1964, Adv. Phys., **13**, 170.
Lu, J. P., T. Odagaki, and J. L. Birman, 1986, Phys. Rev. B **33**, 4809.
Luban, M., and J. H. Luscombe, 1987, Phys. Rev. B **35**, 9045.
Luban, M., J. H. Luscombe, and S. Kim, 1988, Phys. Rev. Lett. **60**, 2689.
Luck, J. M., and D. Petritis, 1986, J. Stat. Phys. **42**, 289.
McKenna, M. J., R. J. Stanley, E. DiMasi, and J. D. Maynard, 1990, Physica B **165**, 603.
McKenna, M. J., R. L. Stanley, and J. D. Maynard, 1992, Phys. Rev. Lett. **69**, 1807.
McKenna, M. J., J. Keat, J. Wang, and J. D. Maynard, 1994, Physica B **194-196**, 1039.
Merlin, R., K. Bajema, R. Clarke, F.-Y. Juang, and P. K. Bhattacharya, 1985, Phys. Rev. Lett. **55**, 1768.
Mermin, N. D., 1980, Bull. Am. Phys. Soc. **33**, 213.
Morse, P. M. and K. U. Ingard, 1968, *Theoretical Acoustics* (McGraw-Hill, New York), pp. 847, 856.
Mott, N. F., 1967, Adv. Phys. **16**, 49.
Niu, Q., and F. Nori, 1986, Phys. Rev. Lett. **57**, 2057.
Onoda, G. Y., P. J. Steinhardt, D. P. DiVincenzo, and J. E. S. Socolar, 1988, Phys. Rev. Lett. **60**, 2653.
Ostlund, S., R. Pandit, D. Rand, H. J. Schellnhuber, and E. D. Siggia, 1983, Phys. Rev. Lett. **50**, 1873.
Ostlund, S., and R. Pandit, 1984, Phys. Lett. B **29**, 1394.
Penrose, R., 1974, Bull. Inst. Math. Appl. **10**, 266.
Scharf, R., Y. S. Kivshar, A. Sanchez, and A. R. Bishop, 1992, Phys. Rev. A **45**, R5369.
Shechtman, D., I. Blech, D. Gratias, and J. W. Cahn, 1984, Phys. Rev. Lett. **53**, 1951.
Sheng, P., 1995, *Introduction to Wave Scattering, Localization, and Mesoscopic Phenomena* (Academic Press, San Diego).
Simon, B., 1982, Adv. Appl. Math. **3**, 463.
Socolar, J. E. S., and P. J. Steinhardt, 1986, Phys. Rev. B **34**, 617.
Sutherland, B., 1986, Phys. Rev. B **34**, 3904.
Weaver, R. L., 1990, Wave Motion **12**, 129.
Ziman, J. M., 1960, *Electrons and Phonons* (Clarendon, London).